POAC'25
St. John's, Newfoundland and Labrador, Canada

Proceedings of the 28th International Conference on Port and Ocean Engineering under Arctic Conditions
Jul 13-17, 2025
St. John's, Newfoundland and Labrador
Canada

Propeller-Ice Interaction experiments on a scaled S.A. Agulhas II Propeller

Angelo Mario Böhm[1], Franz von Bock und Polach[1]
[1] Institute of Ship Structural Design and Analysis (M-10), Hamburg University of Technology (TUHH), Hamburg, Germany

ABSTRACT

Between 2011 and 2020, over 16% more incidents of machinery damage and failure were reported in the waters within the Arctic Circle compared to the rest. In addition, Allianz (AGCS) also reported that machinery damages and failures account for more than 45% of all incidents in Arctic waters, which are caused by the exposure of the propulsion system to ice contact. A better understanding of the propeller-ice interaction process would allow a more efficient propeller design and a safer operation in ice-covered waters. However, full-scale measurements of propeller-ice loads are unique. In addition, propeller-ice loads determined in model tanks are hard to transfer to full scale due to the model ice properties and the large scaling of the propeller. Moreover, holistic propeller-ice simulations have yet to be created, capturing the complex ice failure and representing realistic loads. This paper presents propeller-ice interaction experiments on the propeller of S.A. Agulhas II on a scale of 1:3. The experiments focus on contact milling and impact loads. The test matrix consists of different interaction velocities up to 4 m/s using a drop-tower, cylindrical ice specimen with diameters up to 200 mm, and three different contact conditions from milling loads to impact loads. The specimens consist of granular freshwater ice with high uniaxial strength, and the reports of the measured interaction force and the strains measured on the propeller should provide valuable information for future simulations of the propeller-ice interaction process.

KEY WORDS: Ice; Propeller; Icebreaker; Milling loads; Impact loads

INTRODUCTION

Ice loads on ship hulls have been measured extensively in previous studies (Hoffmann, 1985; Kujala et al., 2009; Suominen et al., 2013; Suominen, 2018) and can be estimated to a certain degree. However, thrust and torque measurements from the intermediate shaft using strain gauges only provide an indication of the propeller-ice load (Suominen et al., 2013; de Waal et al., 2018b; de Waal et al., 2018a). A notable exception is the full-scale instrumentation of the propeller blade on the icebreaker USCGC Polar Star, which employed 54 Fabry-Pérot based

fibre-optic strain gauges and shaft-mounted electronics during measurements in Antarctic waters in December 1994 and January 1995 (Morin et al., 1996). This unique study underscores the need for analytical, numerical, and small-scale experimental investigations into the propeller-ice interaction process.

Propeller-ice loads are commonly classified into contact loads—comprising milling and impact loads—and non-contact loads, such as hydrodynamic loads and hydrodynamic blockage. Milling loads occur when the leading edge of the propeller cuts into the ice, whereas impact loads arise when the ice strikes the propeller face without being cut. Hydrodynamic loads develop in the absence of direct ice contact, while hydrodynamic blockage refers to cases where ice, although not in direct contact, is close enough to influence the flow around the propeller. This work focuses on contact milling and impact loads.

Belyashov (Belyashov, 1993; Belyashov, 1995) investigated ice milling contact and failure mechanics using model edges and suggested extending these experiments to include propeller edges. The ice impact contact mechanism is analogous to a uniaxial compression test of ice, one of the most extensively studied mechanical properties of ice (Timco and Weeks, 2010). Because the compressive properties of ice depend on the applied strain rate, and since the impact speeds in propeller-ice interactions are higher than those in ice-ship-hull interactions, it is necessary to extend the experimental database to higher strain rates.

Recent studies have examined ice milling contact forces and failure patterns using model edges in a compression testing machine at speeds of approximately 0.2 m/s (Böhm et al., 2022) and subsequently in a drop tower at speed of 5 m/s (Böhm et al., 2024). In the present study, the same drop tower is employed with a strain gauge-instrumented 1:3 scaled propeller blade of the S.A. Agulhas II. The combined analysis of the milling and impact interaction forces and the strain response of the propeller blade will provide valuable insights for future simulations of the ice-propeller contact scenario. Furthermore, high-speed recordings of the ice fracture process provide critical insights for the development of advanced numerical ice material models, thereby enhancing the simulation of ice-propeller contact scenarios.

EXPERIMENTS

It follows a description of the ice specimen production and preparation and the experimental setup.

Specimen Production and Preparation

The ice specimens used for the experiments were cylindrical, with a diameter of 200 mm. The ice specimen production process is based on (Gudimetla et al., 2012), but commercial crushed ice was used instead of self-made crushed ice. For the freezing process of the ice specimens, PVC-U pipes were used, which were sealed at the bottom with a thin aluminium plate and insulated at the top. This ensured freezing from bottom to top and avoided cracking during the freezing process. The forms were filled with one third distilled water and two thirds commercially available crushed ice to obtain a granular grain structure of the ice. The ice specimens were prepared and frozen in a refrigerated container at -10 °C. The freezing time was seven days for the ice specimens. After freezing, the ice specimens were removed from the pipes under ambient conditions in the laboratory and again stored in the refrigerated container at -10 °C. The ice specimens were shortened to 200 mm with a bandsaw. Beyond this, the ice specimens did not receive any further treatment.

Experimental Setup

The propeller-ice impact and milling experiments were conducted using a drop tower, achieving interaction velocities of up to 4 m/s and corresponding strain rates of up to 20 s^{-1}. Our project partner, Piening Propeller, manufactured a 1:3 scaled version of the S.A. Agulhas II propeller blade, fabricated from aluminium bronze, and provided the propeller hub. The propeller blade was instrumented with seven strain gauge rosettes. Figure 1 provides an overview of the experimental setup and the blade instrumentation.

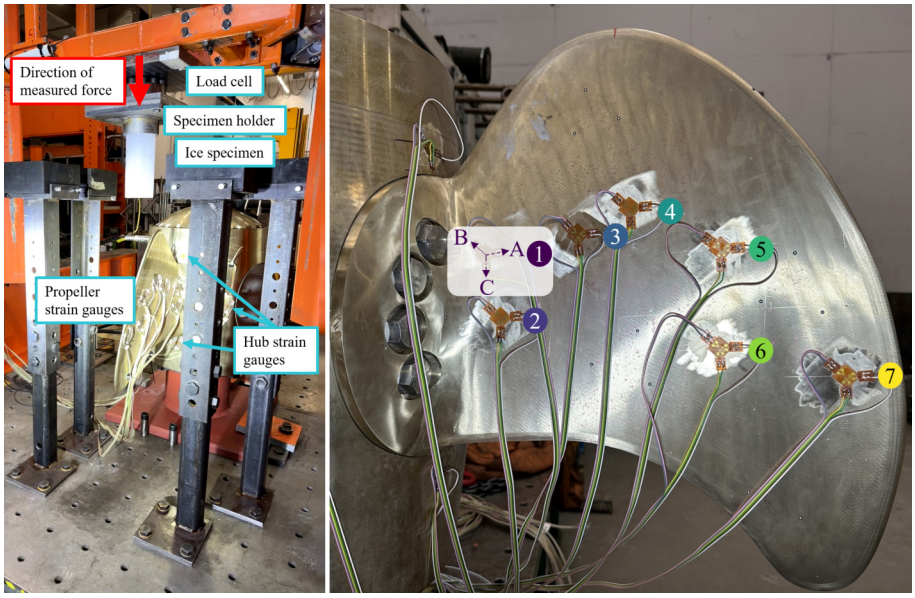

Figure 1: Left: Experimental setup of the propeller-ice impact and milling experiments; Right: Propeller blade instrumentation showing the position of the strain gauge rosettes and the axis orientation.

Ice specimens were mounted onto the drop hammer using a specimen holder capable of accommodating specimens with diameters of 100 mm and 200 mm. An emergency release hook disengaged the vertically guided drop hammer from a predefined height, allowing the ice specimen to impact the propeller blade; the remaining energy was absorbed by shock dampers. The force signal was sampled at 100 kHz, and the strain components of the rosettes were recorded at 20 kHz. The propeller could rotate by approximately 71°, enabling the adjustment of initial contact conditions from impact to milling loads. In addition to the force and strain measurements, high-speed recordings were conducted to capture the fracture mechanisms of the ice during impact. Figure 1 (left) illustrates the experimental setup under milling conditions using a 100 mm diameter ice specimen.

Interaction loads and 21 strain components from the propeller blade and hub were measured during the impact. Figure 1 (right) displays the propeller blade instrumentation, including the A, B, and C-axis orientations of the strain gauge rosettes. The color coding for rosettes 1–7, as shown on the right side of Figure 1, is also used in the Results section.

Due to the limited availability of the propeller hub for testing, the number of repetitions was constrained. Moreover, tests using the smaller 100 mm diameter ice specimens yielded low force and strain responses such that reporting these results would exceed the scope of this paper. Consequently, this paper presents the 29 results obtained from experiments using the 200 mm diameter ice specimens.

RESULTS

It follows a description of the experimental results in the form of the measured ice-propeller contact load histories, the strain measurements on the propeller, and the fracture mechanics in the form of high-speed recordings.

Ice-propeller contact load histories

The presentation of just the individual force-time curves in different colors is transparent yet convolutes the depiction. The Interquartile Range (IQR) present the variability of the measurements, and the mean and the median can summarize the individual curves. Figure 2 shows the force-time curves of the impact test with the ice specimen diameter of 200 mm and an impact velocity of 2 m/s (Figure 2a) and 4 m/s (Figure 2b), showing in grey the individual curves, in blue the mean of the individual curves, and in red the median of the individual curves. The IQR has a transparent red. The IQR accompanied by the median and mean provides a robust and representative summary of the contact load variability in contrast to a min-max representation. Therefore, in the following, only the IQR along with the median and mean is presented for the force-time curves.

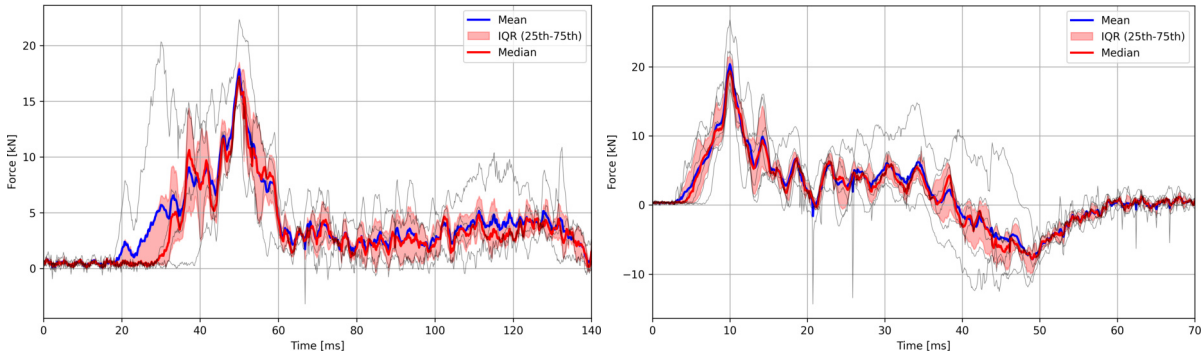

(a) Force-time curves of the impact test at 2 m/s impact velocity; 4 repetitions

(b) Force-time curves of the impact at 4 m/s impact velocity; 6 repetitions

Figure 2: Force-time curves of the impact test with the ice specimen diameter of 200 mm showing mean, median, and IQR at 2 m/s and 4 m/s interaction velocity

Figure 2a shows that the interaction between the ice specimen and the propeller at 2 m/s initial contact velocity takes about 120 ms. The force increases for about 10-30 ms to 14.76 kN – 22.34 kN and drops for 10 ms to level between 2.5 kN – 5 kN. With fluctuations, the level remains constant for 80-90 ms until no interaction is recorded, which can also be seen later in the strain measurements. The peak mean force is 17.88 kN and the peak median force is 17.21 kN. Figure 2b shows that the interaction between the ice specimen and the propeller at 4 m/s initial contact velocity takes the half as long as the interaction at 2 m/s. The force increases for about 5 ms to 16.85 kN – 26.78 kN and drop for 10 ms to 0 kN. After the drop to 0 kN the force increases to a level of about 5 kN for 20 ms following a second drop for 10 ms close to –10 kN. After 10 ms the force increases back to around 0 kN and the interaction between the ice speciemen and the propeller blade ends.
For the next experiments the propeller blade is rotated 35°, which remains an impact type interaction. Figure 3 shows the force-time curves of the 35° impact test with an impact velocity of 2 m/s (Figure 3a) and 4 m/s (Figure 3b).

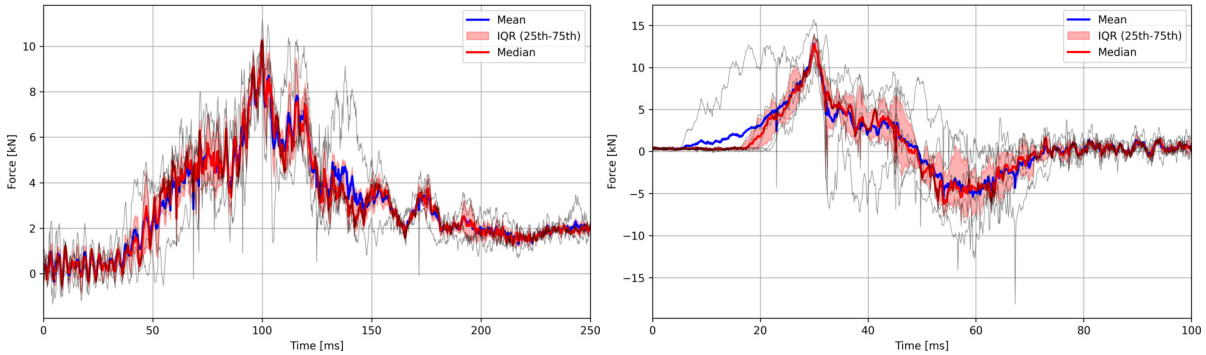

(a) Force-time curves of the 35° impact test at 2 m/s impact velocity; 4 repetitions

(b) Force-time curves of the 35° impact test at 4 m/s impact velocity; 6 repetitions

Figure 3: Force-time curves of the 35° impact test with the ice specimen diameter of 200 mm showing mean, median, and IQR at 2 m/s and 4 m/s interaction velocity

The interaction takes about 150 ms for the tests at an interaction velocity of 2 m/s in the 35° impact condition, see Figure 3a. In the end of the experiment the ice specimen does not fail globally, and the remaining ice specimen is in contact with the propeller and the total weight of 200 kg results in the measured static load (drop hammer including remaining ice specimen). In the beginning of the interaction, the force increases in a saw-tooth pattern for about 60 ms to 9.57 kN – 11.17 kN. For 40 ms the force decreases to 2 kN and bounces for 40-50 ms between 4 kN and 2 kN. Figure 3b shows the force-time curves of the 35° impact test with an impact velocity of 4 m/s. In contrast to the interaction at 2 m/s, the ice specimen fails globally. Thus, the total interaction takes about 50 ms and in the end of the experiment no remaining force is measured. In the beginning of the interaction, the force increases more rapidly for about 10-20 ms to 10.67 kN - 15.72 kN. After the peak, the force decreases for 30 ms to about -10 kN with a subsequent increase to 0 kN after 20 ms.

For the last series of experiments the propeller blade is rotated in total 71° from the initial impact condition. This time the interaction changes from an impact type to a milling type interaction. Figure 4 shows the force-time curves fo the milling tests with a milling velocity of 2 m/s (Figure 4a) and 4 m/s (Figure 4b).

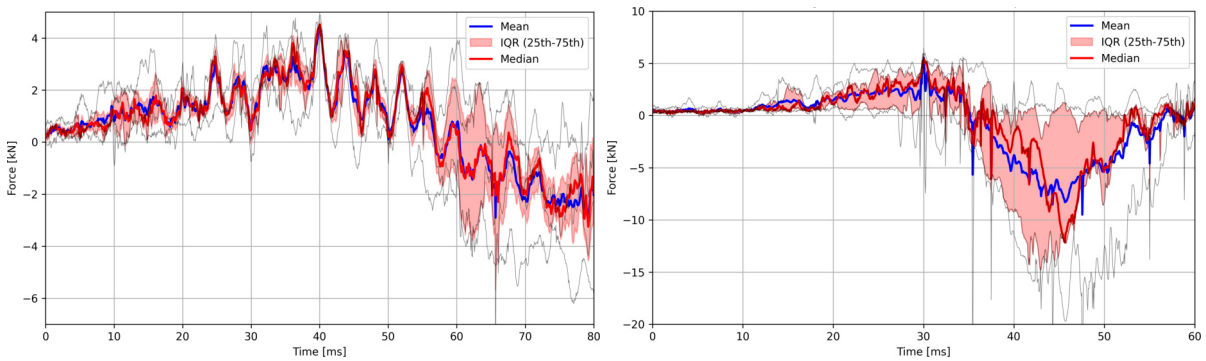

(a) Force-time curves of the milling test at 2 m/s impact velocity; 4 repetitions

(b) Force-time curves of the milling test at 2 m/s impact velocity; 5 repetitions

Figure 4: Force-time curves of the milling test with the ice specimen diameter of 200 mm showing mean, median, and IQR at 2 m/s and 4 m/s interaction velocity

Figure 4a shows that the milling of the ice specimen at an initial interaction velocity of 2 m/s

takes about 60 ms. The force increases in a saw-tooth pattern with larger periods than in the 35° impact test for 40 ms to 4.12 kN - 4.88 kN. After the peak, the force decreases in a saw-tooth pattern for 20 ms below 0 kN. The milling of the ice specimen at an initial interaction velocity of 4 m/s takes about 30 ms, see Figure 4b. The milling force increases for 20 ms to 4.67 kN - 6.45 kN. About five milliseconds after the peak, the measured force drops below 0 kN and the milling interaction ends.

Strain measurements during propeller-ice contact

The von Mises strain, ε_{vm}, was computed from the measured strain components A, B, and C using the following relations:

$$\varepsilon_{1,2} = \frac{\varepsilon_A + \varepsilon_C}{2} \pm \frac{\sqrt{2}}{2}\sqrt{(\varepsilon_A - \varepsilon_B)^2 + (\varepsilon_C - \varepsilon_B)^2}, \tag{1}$$

$$\varepsilon_{vm} = \sqrt{\varepsilon_1^2 + \varepsilon_2^2 - \varepsilon_1\,\varepsilon_2}. \tag{2}$$

The strain gauge rosettes measure normal strains in three directions (A, B, C), from which the in-plane principal strains ε_1 and ε_2 are computed assuming plane stress conditions. The von Mises equivalent strain is then calculated using the standard 2D formulation.
Figure 5 shows the von Mises strain and its strain components at Gauge 1 over time, showing median, IQR, and the A,B,C-strain contributions during an impact test at a velocity of 2 m/s.

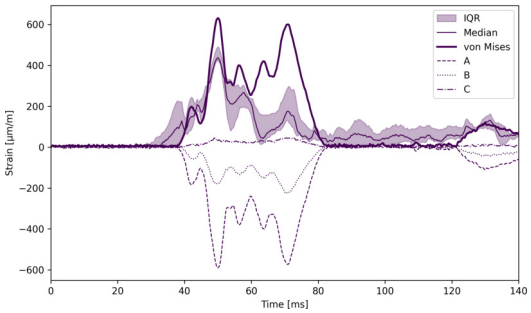

Figure 5: Von Mises strain at Gauge 1 over time, showing median, IQR, and A,B,C-strain contributions during an impact test at a velocity of 2 m/s

The strain component at the A-axis has the largest contribution to the von Mises strain, followed by the strain component at the B-axis, which is about one third of the strain at the A-axis. The strain at the C-axis has nearly no contribution to the von Mises strain. Below, we present the individual von Mises strain responses of the strain gauges rosettes and compare the measurement curves across the different test conditions.
In the impact test at 2 m/s, the strain distributions show significant variation among the gauges, see Figure 6a. Gauge 1 (purple curve) recorded a peak mean von Mises strain of 478.64 μm/m with a median of 437.33 μm/m and a min-max envelope ranging from 408.75 μm/m to 631.16 μm/m. This suggests a pronounced local strain amplification. Gauge 2 exhibited a slightly higher peak mean of 511.00 μm/m and a maximum envelope of 675.16 μm/m, indicating an area of elevated stress. Gauges 3 and 4 showed moderate responses with peak means of 442.18 μm/m and 426.12 μm/m, respectively, and envelope ranges that support a less severe strain field compared to Gauges 1 and 2. Gauges 5 and 6 (green and bright green) yielded lower strain levels with peak means of 321.17 μm/m and 370.54 μm/m. Notably, Gauge 6

displayed a broader min envelope 216.23 μm/m and max envelope 518.05 μm/m, reflecting a more variable response. Gauge 7 (yellow) consistently recorded the lowest values with a peak mean of 118.60 μm/m, indicating a region of minimal strain.
When the interaction velocity is increased to 4 m/s, the strain magnitudes generally rise, see Figure 6b.

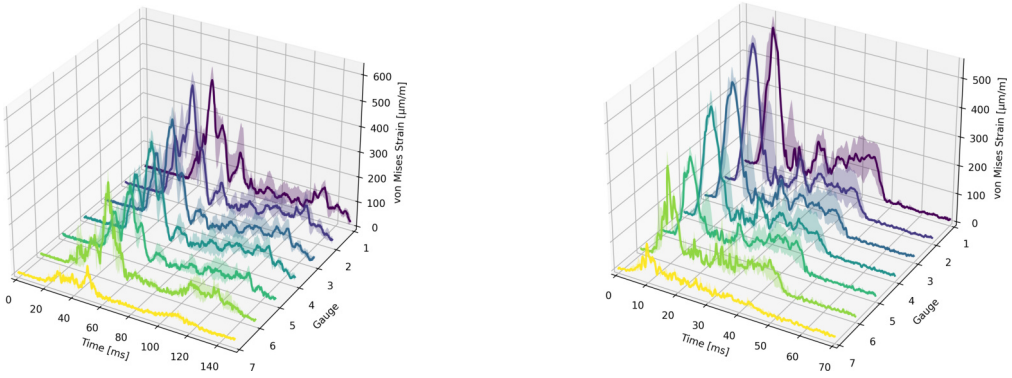

(a) Von Mises strain distribution over time and gauge position during impact tests at 2 m/s; 4 repetitions

(b) Von Mises strain distribution over time and gauge position during impact tests at 4 m/s; 6 repetitions

Figure 6: Median and IQR von Mises strain distribution over time and gauge position during impact tests at 2 m/s and 4 m/s

Gauge 1 shows an increased peak mean of 552.86 μm/m and an expanded envelope from 471.39 μm/m to 778.01 μm/m. Gauge 2 yields a peak mean of 543.31 μm/m with a similar envelope expansion (up to 743.83 μm/m). Gauges 3 and 4 maintain moderate responses with peak means of 473.87 μm/m and 436.84 μm/m, respectively. Gauges 5 and 6 again record lower strain magnitudes, with peak means of 314.83 μm/m and 334.30 μm/m. Gauge 7 remains the least affected, with a peak mean of 128.24 μm/m. Figure 6 indicates that higher velocities amplify the strain response, particularly at regions corresponding to Gauges 1 and 2. For the 35° impact test at 2 m/s, the strain magnitudes decrease compared to the normal impact, see Figure 6a and Figure 7a.

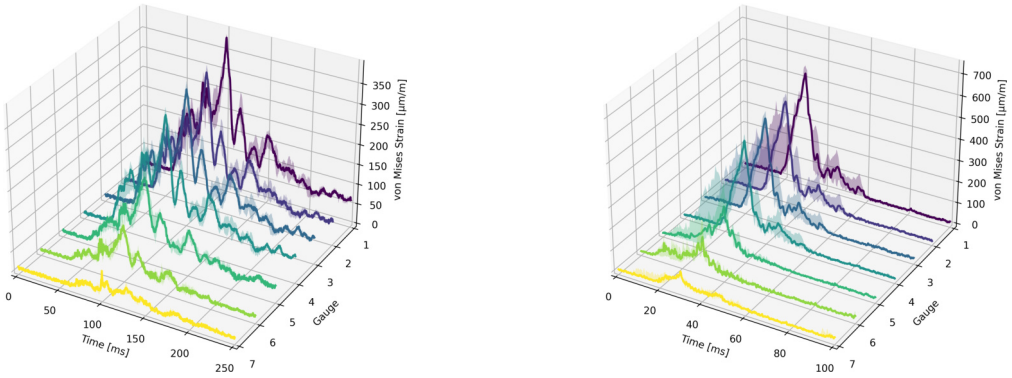

(a) Von Mises strain distribution over time and gauge position during impact tests, propeller rotation of 35°, 2 m/s; 4 repetitions

(b) Von Mises strain distribution over time and gauge position during impact tests, propeller rotation of 35°, 4 m/s; 6 repetitions

Figure 7: Median and IQR von Mises strain distribution over time and gauge position during impact tests, propeller rotation of 35°, at 2 m/s and 4 m/s

In Figure 7a, Gauge 1 shows a reduced peak mean of 377.24 μm/m (min-max envelope: 345.74 μm/m - 397.70 μm/m). Gauge 2 decreases to a peak mean of 341.60 μm/m. Gauges 3 and 4 exhibit peak means of 334.81 μm/m and 313.36 μm/m, respectively. Gauges 5, 6, and 7 show further reduced responses with peak means of 212.56 μm/m, 131.72 μm/m, and 68.90 μm/m.

At 4 m/s in the 35° impact test configuration, strain levels increase relative to the 2 m/s case while preserving the overall distribution. In Figure 7b Gauge 1, registers a peak mean of 547.34 μm/m with a peak maximum of 742.31 μm/m. Gauge 2 records 486.56 μm/m. Gauges 3 and 4 show peak means of 481.29 μm/m and 451.08 μm/m. Gauges 5, 6, and 7 yield intermediate values of 276.90 μm/m, 206.38 μm/m, and 98.57 μm/m, respectively. Figure 6 and Figure 7 highlight the sensitivity of strain levels to both contact condition and interaction velocity.

In Figure 8, the milling tests show substantially lower strain magnitudes, with only minor differences between the two velocities.

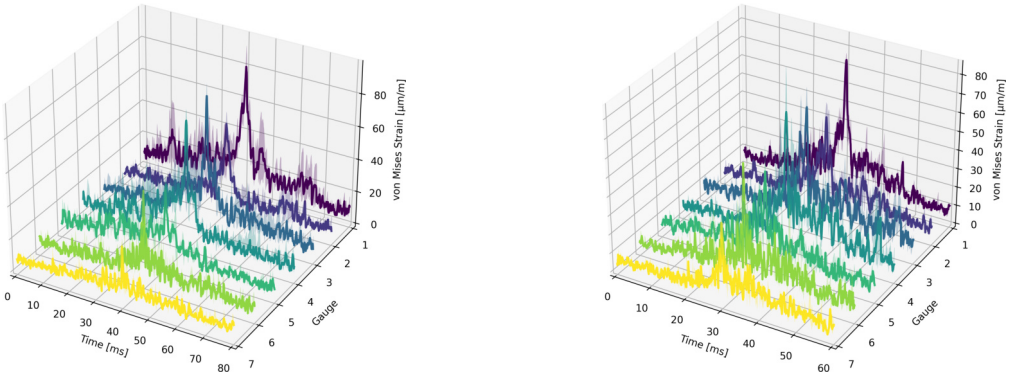

(a) Von Mises strain distribution over time and gauge position during milling tests at 2 m/s; 4 repetitions

(b) Von Mises strain distribution over time and gauge position during milling tests at 4 m/s; 5 repetitions

Figure 8: Median and IQR von Mises strain distribution over time and gauge position during milling tests at 2 m/s and 4 m/s

In Figure 8a, Gauge 1 exhibits a peak mean of only 75.98 μm/m (min-max envelope: 47.34 μm/m - 97.64 μm/m). Gauge 2 records 55.39 μm/m. Gauges 3 and 4 show similar values with peak means of 77.11 μm/m and 75.01 μm/m. Gauges 5, 6, and 7 display the lowest responses with peak means of 48.87 μm/m, 59.85 μm/m, and 35.21 μm/m, respectively.

In the milling test at 4 m/s, the strain levels remain comparably low, see Figure 8b. Gauge 1 shows a slight decrease with a peak mean of 66.27 μm/m. Gauge 2 records 52.58 μm/m. Gauges 3 and 4 yield peak means of 67.80 μm/m and 80.02 μm/m. Gauges 5, 6, and 7 present values of 53.64 μm/m, 59.68 μm/m, and 44.48 μm/m, respectively.

Figure 2–4 and Figure 8 suggest an oscillatory behavior in the force and strain responses. A modal analysis of the propeller blade conducted in LS-DYNA revealed the first eigenfrequencies at approximately 173 Hz and 313 Hz. However, spectral analysis of the strain signals showed no consistent large-amplitude content above 200 Hz in the ensemble mean. Only a few individual test runs exhibited notable spectral peaks beyond this range. This indicates that structural vibrations may occur in isolated cases but are not a dominant feature across all tests. While these observations point to limited structural vibration effects, they raise the question of whether the dynamic response of the blade should be explicitly considered in modeling. This is

further discussed in the Discussion and Conclusion section.

Ice fracture mechanism

Figure 9 depicts the fracture mechanisms observed during the propeller-ice interaction experiments using 200 mm diameter ice specimens. In addition, Figure 9 shows the remaining ice specimen after the propeller-ice impact experiment at 2 m/s under the 35° contact condition (see Figure 9d) as well as after the propeller-ice milling experiment (see Figure 9e). Pictures of the ice fracture process were recorded at frame rates between 5,000 - 10,000 frames per second.

(a) Impact experiment

(b) Impact experiment under the 35° contact condition

(c) Milling experiment

(d) End of impact experiment under the 35° contact condition

(e) End of milling experiment

Figure 9: High-speed recording of the ice fracture during the propeller impact and milling experiments (9a-9c) and pictures of the remaining ice specimen after test execution for the impact experiment under the 35° contact condition (9d) and the milling experiments (9e)

The ice impact experiments are characterized by local crushing at the contact location and the development of perpendicular cracks, which vary with the initial contact condition (see Figures 9a–9b). Figure 9b shows the ice fracture in the 35° contact condition at 4 m/s. As previously reported in the section on propeller-ice contact load histories, an initial interaction velocity of 2m/s under the 35° contact condition was insufficient to fracture the ice specimen. Figure 9d illustrates the loading of the propeller blade by the remaining ice specimen together with the drop hammer at the end of the experiment, which is also reflected by the force measurements (see Figure 3a). The high-speed recordings further revealed rotation of the propeller during tests under the 35° contact condition, whereas in the standard impact and milling conditions the propeller blade position remained stable. Figure 9c shows the fracture of the ice specimen during the milling interaction, which is characterized by local crushing followed by the break-off of ice wedges on both sides. Finally, Figure 9e displays the remaining ice specimen after the milling experiment and the protective cover for the strain gauges, ensuring that the gauges were not impacted by flying ice debris.

Discussion and Conclusion

A detailed analysis of the force-time curves reveals differences between the various contact conditions. For the 2 m/s impact tests, the interaction lasts approximately 120 ms, with the force increasing over 10–30 ms to peak values between 14.76 kN and 22.34 kN before dropping briefly and then stabilizing. At 4 m/s, the interaction duration is halved, and the force

profile exhibits a rapid rise to 16.85–26.78 kN, followed by a transient drop and subsequent fluctuations. The 35° impact tests demonstrate that at 2 m/s the interaction lasts about 150 ms, with a saw-tooth force pattern indicating intermittent loading, while at 4 m/s the ice specimen fails globally within roughly 50 ms, terminating the force transmission. Milling tests at 2 m/s and 4 m/s exhibit interaction duration of approximately 60 ms and 30 ms, respectively, with corresponding saw-tooth force profiles.

While these force histories suggest limited high-frequency content, isolated oscillations were observed. Spectral analysis and modal simulation indicate that the propeller's dynamic response, although not dominant in most cases, may still play a role under specific conditions. For future modeling efforts, particularly at higher speeds or with more flexible geometries, incorporating structural dynamics may help to better capture transient blade responses.

The interquartile range (IQR) improves upon a simple min-max envelope by constraining the data more effectively for subsequent numerical simulations. Additionally, an unexpected rotation of the propeller during the 35° impact tests—likely due to imperfections in the hydraulic system—resulted in non-linear movement, complicating the direct use of these results in simulation models.

The experimental results also reveal differences in both the magnitude and spatial distribution of von Mises strains measured on the propeller blade between the various contact conditions. In impact tests, the spatial strain gradient is pronounced, with the rosettes near the propeller blade root (Gauges 1 and 2) generally recording the highest von Mises strains. Notably, in both the 2 m/s and 35° impact tests at 2 m/s, instances occur where Gauge 2 registers higher strain than Gauge 1. In contrast, milling tests produce considerably lower strain magnitudes with a more uniform distribution across the propeller surface.

Moreover, high-speed recordings of the ice fracture mechanism, combined with the strain response of the propeller and the interaction force measurements, offer a comprehensive dataset that is instrumental in developing numerical ice material models capable of accurately representing the complex propeller-ice contact loads.

In summary, our experimental investigations confirm that impact tests induce higher and more variable von Mises strains compared to milling tests, and that increasing interaction velocity amplifies these effects. These findings, along with the detailed load histories, provide critical insights for refining numerical ice material models and enhancing simulations of propeller-ice interactions.

ACKNOWLEDGEMENTS

The authors would like to acknowledge support from MarTERA - an ERA-NET Cofund scheme of Horizon 2020 of the European Commission - and the Research Council of Norway (Project no. 311502), the Federal Ministry for Economic Affairs and Climate Action of Germany (Project no. 03SX519B), and Department of Science and Technology of South Africa, through the HealthProp project. It is stated that the funder is not responsible for any of the content of this publication. The authors would also like to express their gratitude to Andrzej Iwaszko, Lina Sapp, Jorrid Lund, and Franciska Müller for their valuable support and contributions to this work.

REFERENCES

Belyashov, V. A. (1993). An investigation on fracture mechanics and ice loads during cutting freshwater ice by indenters simulating propeller blades. part 1: Flat horizontal indenters. In

International Conference on Port and Ocean Engineering under Arctic Conditions, pages 3–16.

Belyashov, V. A. (1995). An investigation on fracture mechanics and ice loads during cutting freshwater ice by indenters simulating propeller blades. part 2: Flat vertical indenters. In *International Conference on Port and Ocean Engineering under Arctic Conditions*, pages 18–30.

Böhm, A. M., Herrnring, H., and von Bock und Polach, F. (2022). Splitting-tests of laboratory-made granular ice with a propeller-like indenter. In *Volume 6: Polar and Arctic Sciences and Technology*. American Society of Mechanical Engineers.

Böhm, A. M., Sapp, L., and von Bock und Polach, F. (2024). Derivation of a numerical propeller-ice interaction model. In *8th International Symposium on Marine Propulsors (smp 2024)*. Norwegian University of Science and Technology, Department of Marine Technology.

de Waal, R. J. O., Bekker, A., and Heyns, P. S. (2018a). Data for indirect load case estimation of ice-induced moments from shaft line torque measurements. *Data in brief*, 19:1222–1236.

de Waal, R. J. O., Bekker, A., and Heyns, P. S. (2018b). Indirect load case estimation for propeller-ice moments from shaft line torque measurements. *Cold Regions Science and Technology*, 151:237–248.

Gudimetla, P. S. R., Colbourne, B., Daley, C., Bruneau, S. E., and Gagnon, R. (2012). Strength and Pressure Profiles of Conical Ice Crushing Experiments. In *Day 2 Tue, September 18, 2012*. SNAME.

Hoffmann, L. (1985). Impact forces and friction coefficent on the forebody of the german polar research vessel polarstern. In *International Conference on Port and Ocean Engineering under Arctic Conditions: 1985*.

Kujala, P., Jiang, Z., Li, F., and Lu, L. (2009). Long term prediction of local ice loads on the hull of s.a. agulhas ii. In *International Conference on Port and Ocean Engineering Under Artic Conditions. 2009*. Lulea University of Technology.

Morin, A., Caron, S., van Neste, R., and Edgecombe, M. H. (1996). Field monitoring of the ice load of an icebreaker propeller blade using fiber optic strain gauges. In Murphy, K. A. and Huston, D. R., editors, *Smart Structures and Materials 1996: Smart Sensing, Processing, and Instrumentation*, SPIE Proceedings, pages 427–438. SPIE.

Suominen, M. (2018). *Uncertainty and variation in measured ice-induced loads on a ship hull*. PhD thesis, Aalto University.

Suominen, M., Karhunen, J., Bekker, A., Kujala, P., Elo, M., von Bock und Polach, F., Enlund, H., and Saarinen, S. (2013). Full-scale measurements on board psrv s.a.agulhas ii in the baltic sea. In *The 22nd International Conference on Port and Ocean Engineering under Arctic Conditions*.

Timco, G. W. and Weeks, W. F. (2010). A review of the engineering properties of sea ice. *Cold Regions Science and Technology*, 60:107–129.